Murine malaria parasite sequestration: CD36 is the major receptor, but cerebral pathology is unlinked to sequestration

Blandine Franke-Fayard*†, Chris J. Janse*†, Margarida Cunha-Rodrigues‡, Jai Ramesar*, Philippe Büscher§, Ivo Que¶, Clemens Löwik¶, Peter J. Voshol¶, Marion A. M. den Boer¶, Sjoerd G. van Duinen‖, Maria Febbraio, Maria M. Mota‡, and Andrew P. Waters*††**

Departments of *Parasitology, ¶Endocrinology and Metabolic Diseases, and ‖Pathology, Leiden University Medical Center, 2300 RC, Leiden, The Netherlands; ‡Instituto Gulbenkian de Ciência, P-2781-901 Oeiras, Portugal; §Department of Parasitology, Prince Leopold Institute of Tropical Medicine, B-2000 Antwerp, Belgium; and **Department of Cell Biology, Lerner Research Institute, Cleveland, OH 44195

Edited by Diane E. Griffin, Johns Hopkins Bloomberg School of Public Health, Baltimore, MD, and approved June 22, 2005 (received for review April 30, 2005)

Sequestration of malaria-parasite-infected erythrocytes in the microvasculature of organs is thought to be a significant cause of pathology. Cerebral malaria (CM) is a major complication of *Plasmodium falciparum* infections, and PfEMP1-mediated sequestration of infected red blood cells has been considered to be the major feature leading to CM-related pathology. We report a system for the real-time *in vivo* imaging of sequestration using transgenic luciferase-expressing parasites of the rodent malaria parasite *Plasmodium berghei*. These studies revealed that: (*i*) as expected, lung tissue is a major site, but, unexpectedly, adipose tissue contributes significantly to sequestration, and (*ii*) the class II scavenger-receptor CD36 to which PfEMP1 can bind is also the major receptor for *P. berghei* sequestration, indicating a role for alternative parasite ligands, because orthologues of PfEMP1 are absent from rodent malaria parasites, and, importantly, (*iii*) cerebral complications still develop in the absence of CD36-mediated sequestration, dissociating parasite sequestration from CM-associated pathology. Real-time *in vivo* imaging of parasitic processes may be used to evaluate the molecular basis of pathology and develop strategies to prevent pathology.

imaging | *Plasmodium* | *P. berghei* | luciferase | real-time *in vivo* imaging

Infected red blood cells (irbc) of many species of malaria parasites adhere to the endothelial cells of the microvasculature of numerous deep tissues (1, 2). Termed sequestration, this characteristic may facilitate parasite multiplication, avoiding removal of the irbc by the spleen (3, 4). In some parasite–host combinations, the process of sequestration is associated with pathogenesis, for example, *Plasmodium falciparum* in humans (1, 2, 5) and *Plasmodium berghei* in certain mouse strains (6, 7). Cerebral malaria (CM) is a major complication of *P. falciparum* infections, and the sequestration of irbc has been considered to be the major feature leading to CM-related pathology. Sequestration may lead to vascular obstruction, local endothelial cell activation, and the release of proinflammatory cytokines, resulting in damage to adjacent tissues (2, 7, 8). In *P. falciparum*, the class II scavenger receptor CD36 is a major endothelial receptor. CD36 is involved in not only the adherence of irbc (1, 9, 10) through specific domains of the surface variant antigen PfEMP-1 but also in the modulation of innate and adaptive immune responses (11, 12). To date, most investigations of the dynamics of irbc–receptor interactions rely on *in vitro* observations with cultured cells and immobilized receptors (2). Despite the increase in knowledge of the molecules involved in the binding of irbc to endothelial cells, the specific interactions that lead to pathology have yet to be established. Infection with *P. berghei* in laboratory rodents is a well established model for the investigation of associations among CM, proinflammatory cytokines, and endothelial receptors involved in the sequestration of irbc, leukocytes, and platelets (6, 7). In this study, we developed a method for real-time *in vivo* visualization of the dynamics of the sequestration of *P. berghei* irbc in live hosts. This study generates unexpected insights into sites of sequestration and reports that *P. berghei* sequestration, mediated by CD36, is not the basis for murine CM.

Materials and Methods

Generation of Transgenic *P. berghei* Lines Expressing a GFP-Luciferase Fusion Protein. To introduce GPF-Luciferase into the genome of *P. berghei* parasites, three different constructs were made: p*Pbgfp-luc*$_{CON}$, p*Pbgfp-luc*$_{SCH}$, and p*Pbgfp-luc*$_{GAM}$, in which GFP-luciferase is under the control of three different promoters. Maps and DNA sequences of the described plasmids are available at www.lumc.nl/1040/research/malaria/malaria.html. For detailed information about the construction of the plasmids, see *Supporting Materials and Methods*, which is published as supporting information on the PNAS web site. After linearization at the unique ApaI and KspI sites, the three vectors can integrate into the *ssu-rrna* gene of either the *c-* or the *d-rrna* gene unit by a single crossover event. The three vectors were introduced into wild-type *P. berghei* parasites (reference clone cl15cy1 of the ANKA strain of *P. berghei*). Transfection, selection, and cloning of the transgenic parasites were performed as described in ref. 13, and the following lines that express GFP-luciferase were selected for further analysis: PbGFP-LUC$_{CON}$ (exp 222cl1), PbGFP-LUC$_{SCH}$ (exp 354cl4), and PbGFP-LUC$_{GAM}$ (exp 466, uncloned). To demonstrate correct integration of the vectors into the genome, genomic DNA was isolated from the transgenic parasites and analyzed by Southern analysis, as shown in Fig. 6, which is published as supporting information on the PNAS web site.

Synchronized Blood Stage Development of Transgenic Parasites *in Vitro* and *in Vivo* and Asynchronous Infections *in Vivo*. The following animals (all from Charles River Breeding Laboratories) were infected with the transgenic parasite lines: Swiss mice (male/female, 6 weeks old); C57BL/6 (females, 6 weeks old); BALB/c (female, 6 weeks old); Wistar rats (female, 11 weeks old); Spontaneous Hypertensive (SHR)/NCrlBR rats (female, 8 weeks old) deficient in CD36 expression (14, 15); Wistar–Kyoto (WKY)/NCrlBR rats (female, 8 weeks old) that serve as control for the SHR rats with normal CD36 expression; CD36-null C57BL/6 (CD36$^{-/-}$)

This paper was submitted directly (Track II) to the PNAS office.

Abbreviations: CM, cerebral malaria; irbc, infected red blood cell.

†B.F.-F. and C.J.J. contributed equally to this work.

††To whom correspondence should be addressed at: Department of Parasitology, University of Leiden Medical Center, P.O. Box 9600, 2300 RC, Leiden, The Netherlands. E-mail: waters@lumc.nl.

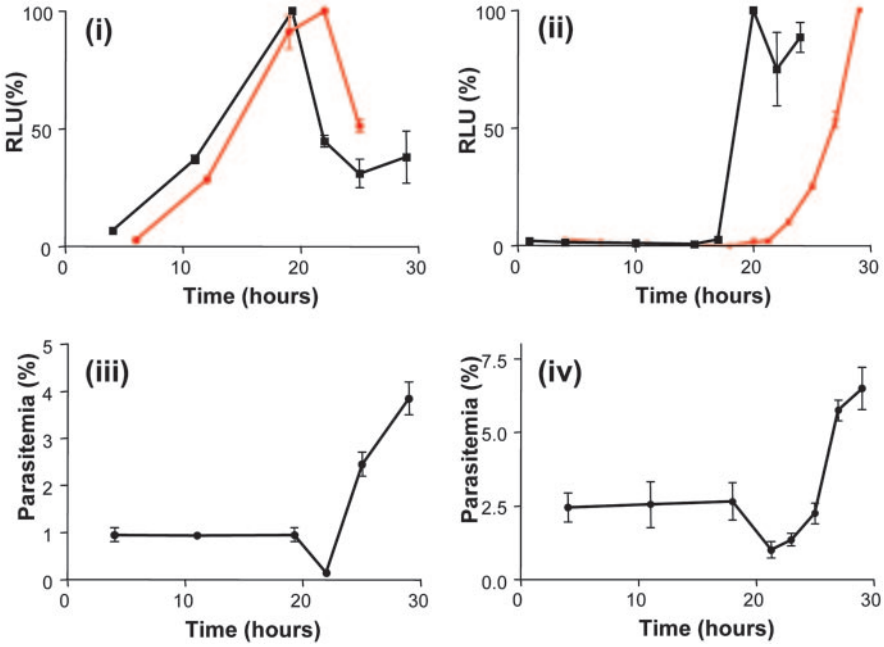

Fig. 1. Analysis of luciferase expression in blood stages. Luciferase expression (RLU%, percentage of relative luminescence) of the blood stages during synchronized blood-stage development *in vitro* and *in vivo* of PbGFP-LUC$_{CON}$ (*Left*) and PbGFP-LUC$_{SCH}$ (*Right*). (*i* and *ii*) Black lines indicate luciferase expression during one cell cycle (24 h) *in vitro*. In PbGFP-LUC$_{CON}$, expression starts in young trophozoites (10 h), peaks in old trophozoites/young schizonts (16–20 h), and decreases in mature schizonts (24 h). In PbGFP-LUC$_{SCH}$, expression occurs exclusively in maturing schizonts (20–24 h). Red lines, luciferase expression in the tail blood of mice during the first 30 h after the injection of merozoites. In PbGFP-LUC$_{CON}$, the decrease at ≈20 h is the result of the disappearance of the schizonts from the blood circulations (*iii*). In PbGFP-LUC$_{SCH}$, activity is observed only after 24 h, when newly invaded young ring stages are present (*iv*) that still show luciferase activity from expression in the schizonts. (*iii* and *iv*) Course of parasitemia in tail blood during the first 30 h after injecting merozoites. The drop in parasitemia at 18–22 h results from the disappearance of the schizonts from the peripheral circulation, and the increase after 24 h results from the presence of newly invading ring forms.

mice (female, 8–16 weeks old) deficient in CD36 expression (16, 17); wild-type control CD36$^{+/+}$ C57BL/6 littermates of the CD36$^{-/-}$ mice (female, 8–16 weeks old); and *Grammomys surdaster* (male/female, 6–12 weeks old), obtained from a breeding colony at the Institute of Tropical Medicine (Antwerp) (18). Synchronized infections of *P. berghei* in rodents (*in vivo*) and synchronized *in vitro* cultures were established as described in refs. 19 and 20; and see *Supporting Materials and Methods*. Asynchronous *in vivo* infections in mice are established by i.p. injection of 10^5–10^6 irbc. Usually, the onset of cerebral complications is determined by measuring the onset and extent of reduction in body temperature on days 5–10 after infection. A drop in temperature to <34°C is indicative of cerebral complications (21, 22). In addition, cerebral complications in the CD36$^{-/-}$ C57BL/6 mice were monitored by ataxia, paralysis, deviation of the head, and convulsions, symptoms leading to coma and death (23). Determination of parasitemia and the percentages of the different parasite stages were performed by counting parasites in Giemsa-stained thin blood films (see *Supporting Materials and Methods*). Purified mature gametocytes of PbGFP-LUC$_{GAM}$ were obtained by using the method described in ref. 24. Erythrocytes (10^8) containing gametocytes were intravenously injected into the tail veins of Swiss mice, resulting in infections, with 0.5–1% of the erythrocytes containing a gametocyte.

Analysis of Stage-Specific Expression of GFP and Luciferase in Blood Stages. GFP fluorescence in the different blood stages of live parasites was visualized by using the GFP filter settings of a Leica fluorescence HC microscope (magnification, ×400), and pictures were recorded with a Hamamatsu ORCA-ER digital camera. To measure luciferase activity of blood stages from infections in rodents, samples (10 μl, in duplicate) of tail blood were collected from synchronized infections at different time points after the injection of purified schizonts. Samples were collected in heparinized tubes and frozen in Eppendorf tubes at −20°C until analysis. To measure the luciferase activity of parasites, 1-ml samples from *in vitro* cultures containing 1–3 × 10^6 parasites were collected (in duplicate), pelleted by centrifugation, and stored at −20°C. Just before analysis, the samples were thawed at room temperature and processed according to the protocol of the Promega Luciferase Assay system. Luminescence spectra of the samples were measured by using a multilabel plate reader (Wallac 1420 Workstation with VICTOR^{2}V; software, PerkinElmer).

Visualization and Quantification of Luciferase Activity in Whole Bodies or Dissected Organs of Infected Animals. Luciferase activity in animals was visualized through the imaging of whole bodies or dissected organs by using an intensified-charge-coupled device (I-CCD) photon-counting video camera of the *in vivo* Imaging System (IVIS 100, Xenogen). Details of the experimental protocols are given in *Supporting Materials and Methods*. Visualization of luciferase activity in animals with synchronous infections was performed at different time points within 30 h after the injection of purified schizonts (for a description of synchronous infections, see above). The time point of 22 h, when most parasites are developing schizonts that disappear from the peripheral blood circulation (see Fig. 1), was used as a reference time point to visualize and quantify sequestration. Luciferase activity in asynchronous infections was usually determined between midnight and 4 a.m. In asynchronous infections of *P. berghei*, development of the parasites is partly synchronous, with the largest proportion of parasites (60–80%) reaching the schizont stage between midnight and 4 a.m. The quantification of luciferase activity in individual organs was performed by using whole organs dissected at 22 h after infection in synchronous infections or at 2 a.m. (on days 4 and 7 after infection) in asynchronous infections. Measurements were done by using

fixed time and region-of-interest settings with the programs LIVING IMAGE (Xenogen) and IGOR PRO (WaveMetrics). Relative photon counts from intact organs were related to the total relative photo counts of all organs.

Visualization of Sequestration of Schizonts in Organs by Using Standard Histological Methods. To visualize the sequestration of schizonts by histological methods, organs were dissected from animals with synchronous infections at 22 h after the injection of purified schizonts or from animals with asynchronous infections at 2 a.m. (see above). The dissected organs were fixed in 4% phosphate-buffered paraformaldehyde for 24–72 h, dehydrated, and paraffin-embedded. Slides of 3 μm were Giemsa-stained and analyzed by light microscopy (magnification, ×1,000) or by polarization microscopy (magnification, ×660).

Results

***In Vivo* Visualization of Sequestration in Rodents by Using *P. berghei* GFP-Luciferase Transgenic Lines.** For the *in vivo* visualization of irbc sequestration, we generated two transgenic lines of *P. berghei*, PbGFP-LUC$_{CON}$ and PbGFP-LUC$_{SCH}$, which express the cytoplasmic fusion protein GFP-luciferase under the control of the constitutive *pbeef1aa* promoter and the schizont-specific *pbama1* promoter, respectively (see Fig. 6 *A* and *B*, which is published as supporting information on the PNAS web site). GFP-luciferase expression was first determined during synchronous blood stage development *in vitro* by measuring luciferase activity (Fig. 1) and monitoring GFP fluorescence (data not shown) during the 22- to 24-h cell cycle of the blood stages. PbGFP-LUC$_{CON}$ expresses GFP-luciferase in all blood stages, is low in ring forms, and peaks in old trophozoites/young schizonts (16–22 h). PbGFP-LUC$_{SCH}$ expresses GFP-luciferase specifically in the schizont stage (20–24 h) and is carried through into young ring stages. To measure the luciferase expression of blood stages *in vivo*, standardized synchronous infections were established by injecting purified merozoites intravenously into animals (20). In these infections, ring-stage parasites are present at 4 h after infection, with a parasitemia between 0.5% and 3%. These ring forms develop within 16–18 h into mature trophozoites that disappear from the blood circulation and sequester at the time of the first nuclear divisions in the schizont stage (see the drop in parasitemia at ≈18 h, shown in Fig. 1) (19). At 22 h, the first newly invaded merozoites of the second asexual cell cycle appear in the blood circulation, and the subsequent invasion of merozoites results in an increase of the parasitemia between 24 and 30 h (Fig. 1). Luciferase activity in samples of the peripheral tail blood of infected animals confirms the *in vitro* luciferase-expression patterns of the two transgenic lines and demonstrates the absence of the schizont stage in the peripheral blood circulation, as shown by the low activities between 18 and 22 h (Fig. 1). To visualize the distribution of the blood stages in animals, we measured the luciferase activity in whole bodies of live animals and in dissected organs by using a photon-counting I-CCD video camera during the 30-h period after the injection of purified merozoites. We first visualized the blood stages of PbGFP-LUC$_{CON}$, which expresses GFP in both nonsequestering trophozoites (10–18 h) and sequestering schizonts (18–22 h). Between 10 and 18 h, luciferase activity is detected throughout the whole body and in all organs, with relatively high activities in the spleen and other organs that contain a large volume of blood, such as heart, lungs, and liver (Fig. 2*A*, 11 h). This distribution of the luciferase activity of nonsequestering stages was confirmed by measuring mice injected with purified mature gametocytes (PbGFP-LUC$_{GAM}$), which express GFP-luciferase specifically in male gametocytes that do not sequester and remain in the circulation (Fig. 2*B*). During the subsequent sequestration period of the schizonts of PbGFP-LUC$_{CON}$ (18–22 h), the activity decreases in organs such as heart and liver, whereas a strong increase is observed in the spleen and lungs and in the lower belly (Fig. 2, 19–22 h). The high signal in the lower belly results from

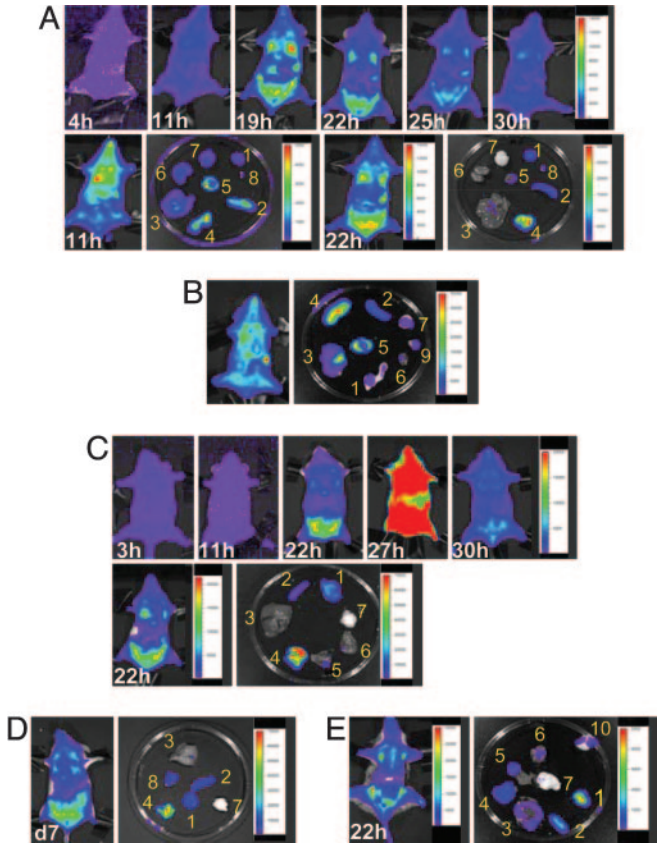

Fig. 2. Visualization of the distribution of luciferase-expressing parasites in live rodents and isolated organs. The distribution of parasites was visualized by measuring luciferase activity in live animals and dissected organs by using an I-CCD video camera. Rainbow images show the relative level of luciferase activity ranging from low (blue), to medium (green), to high (yellow, red). Note that the scale of total photon counts and the time of exposure can be different within separate illustrations. In synchronous infections, measurements were performed at different time points (h, hour) after the injection of purified merozoites. In asynchronous infections, measurements were performed between midnight and 4 a.m. on different days (d) after the injection of 10^5-10^6 parasites. 1, adipose tissue; 2, spleen; 3, liver; 4, lungs; 5, heart; 6, kidneys; 7, brain; 8, mammary fat pad; 9, muscles; and 10, testis; see also Fig. 7. (*A*) Synchronous infection of PbGFP-LUC$_{CON}$ in Swiss mice (60 s). (*B*) A Swiss mouse 5 h after injection with nonsequestering gametocytes of PbGFP-LUC$_{GAM}$ (60 s). (*C*) Synchronous infection of PbGFP-LUC$_{SCH}$ in Swiss mice [(*Upper* 10 s) and (*Lower* 60 s)]. (*D*) Asynchronous infection of PbGFP-LUC$_{SCH}$ in a Swiss mouse at day 7 after infection, just before cerebral complications start (30 s for whole body and 10 s for organs). (*E*) Synchronous infection of PbGFP-LUC$_{SCH}$ in *G. surdaster* (30 s for whole body and 60 s for organs).

schizont sequestration in adipose tissue (Fig. 3; and see below). The patterns of irbc sequestration were analyzed with greater specificity by using the PbGFP-LUC$_{SCH}$ parasites, because these parasites express luciferase only in the schizont stage, thereby avoiding the background activity of nonsequestering stages such as trophozoites and gametocytes. In different mouse and rat strains, luciferase activity was, again, specifically detected in the spleen, lungs, and adipose tissue (Fig. 2*C*; and see Fig. 7, which is published as supporting information on the PNAS web site). Just after the rupture of the schizonts and invasion of new erythrocytes (27 h), the luciferase activity of the ring-stage parasites is detected throughout the whole body (Fig. 2*C*). Luciferase activity was not detected in brain tissue during schizont sequestration (Fig. 2*C*). To investigate whether the observed sequestration pattern was occurring only in our artificially induced synchronous infections, sequestration patterns were analyzed during asynchronous blood-stage infections

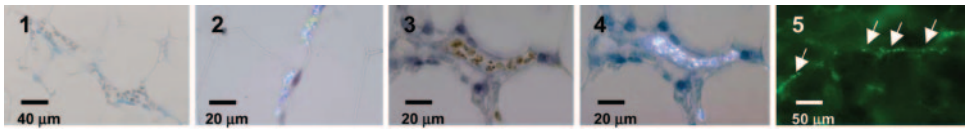

Fig. 3. Visualization of sequestration of schizonts in adipose tissue. Visualization of sequestered schizonts in paraformaldehyde-fixed sections (3 μm) of adipose tissue (from belly fat) of Swiss mice (*1*, *3*, and *4*) and *G. surdaster* (*2*). Representative sections of adipose tissue are shown from animals at 22 h after the injection of purified schizonts (PbGFP-LUC$_{SCH}$), when the sequestration of schizonts occurs. Schizonts are visualized by Giemsa staining (*1*, *3*) or by polarization microscopy (*2*, *4*), demonstrating the characteristic pigment clusters of schizonts that show a marked birefringence by polarization microscopy (magnification, ×660). (*5*) The presence of GFP-expressing sequestered schizonts (arrows) are shown in unfixed adipose tissue of Swiss mouse (magnification, ×400); see also Fig. 8.

(resembling the natural infection), including late-stage infections with cerebral complications (days 5–10 after infection). Schizont accumulation in the lungs, spleen, and adipose tissue was comparable to that of synchronized parasites (Figs. 2*D* and 7) and an increase of luciferase activity in the brains of mice just before and during cerebral complications was never detected. Moreover, in synchronous and asynchronous infections in *G. surdaster*, the natural host of *P. berghei*, schizonts accumulated in the spleen, lungs, and adipose tissue, confirming the relevance of the pattern of sequestration in the laboratory models used (Figs. 2*E* and 7). Accumulation of the schizonts in the capillaries of the spleen, lungs, and adipose tissue, and their absence from other organs, was confirmed by standard histological examination (Fig. 3; and see Fig. 8, which is published as supporting information on the PNAS web site).

***In Vivo* Visualization of *P. berghei* GFP-Luciferase-Sequestering Schizonts in Synchronous Infections in CD36$^{+/+}$ and in CD36$^{-/-}$ C57BL/6 Mice.** CD36 (fatty acid translocase) is a scavenger receptor widely distributed on endothelial cells and a major binding receptor for irbc in several *Plasmodium* species, including *P. falciparum*. We investigated whether CD36 might play a role in the accumulation of *P. berghei* schizonts in the spleen, lungs, and adipose tissue by measuring the luciferase activity of PbGFP-LUC$_{SCH}$ parasites in CD36-deficient SHR rats and CD36-deficient C57BL/6 mice (14, 16). In CD36-deficient animals, sequestration in the adipose and lung tissues was reduced to the same level as that in tissues that do not support schizont sequestration, and parasite accumulation was observed in only the spleen (Fig. 4; and see Fig. 9, which is published as supporting information on the PNAS web site). Furthermore, the absence of CD36 results in a significant increase of schizonts in the peripheral blood circulation (Figs. 4 and 5) and of luciferase activity in the spleen (Figs. 4 and 5), probably reflecting increased irbc clearance. The absence of significant sequestration of schizonts in adipose and lung tissue in the CD36-deficient animals was confirmed by standard histological examination of tissues of the different organs (see Figs. 10 and 11, which are published as supporting information on the PNAS web site). These results show that CD36 is a major receptor for the sequestration of *P. berghei* schizonts in both adipose and lung tissues.

Cerebral Complications and Sequestration of *P. berghei* in Asynchronous Infections in CD36$^{+/+}$ and in CD36$^{-/-}$ C57BL/6 Mice. *P. berghei* causes CM in several laboratory mouse strains, without significant sequestration of irbc in brain tissue (7, 25). To investigate whether the CD36-mediated sequestration plays a role in CM, we determined cerebral complications in CD36$^{-/-}$ C57BL/6 mice. Both wild-type CD36$^{+/+}$ and CD36$^{-/-}$ mice developed neurological symptoms (ataxia, deviation of the head, paralysis, convulsions, and coma) and died 5–10 days postinfection with CM (Fig. 5*A*). CD36$^{-/-}$ mice consistently had a slightly lower parasitemia throughout infection and increased numbers of schizonts in the circulation (Fig. 5*B*). Visualizing the luciferase activity throughout infection until the onset of CM symptoms confirmed the absence of sequestration in brain tissue in both wild-type and CD36$^{-/-}$ mice, the absence of sequestration in lung and adipose tissue in CD36$^{-/-}$ mice (Fig. 5*C*; and see Fig. 12, which is published as supporting information on the PNAS

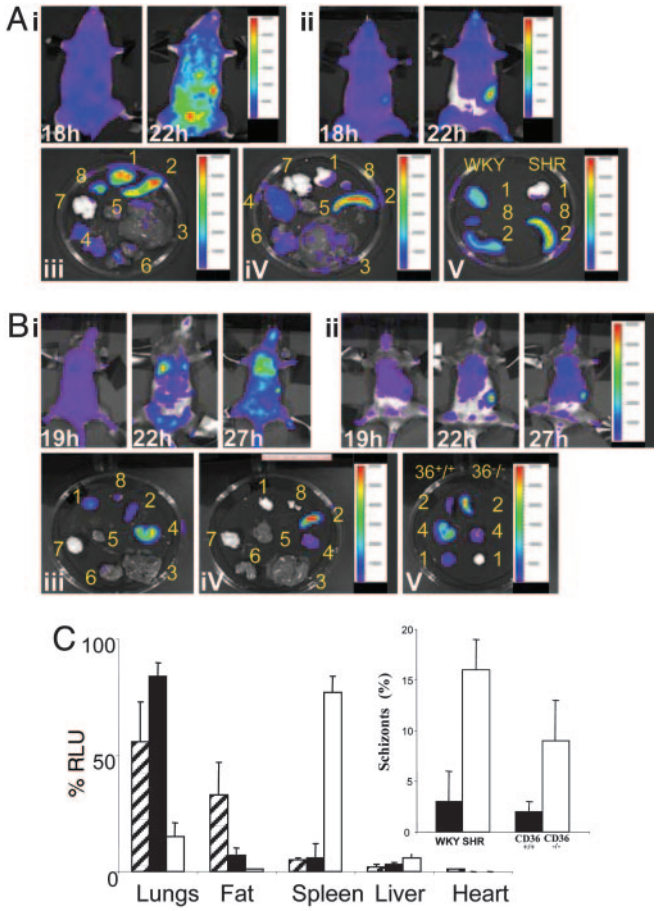

Fig. 4. Visualization and quantification of the sequestration of *P. berghei* in synchronized infections in CD36-deficient rodents. The distribution of schizonts (PbGFP-LUC$_{SCH}$) was visualized by measuring luciferase activity in live animals and dissected organs by using an I-CCD video camera. Measurements were performed at different time points (h, hour) after the injection of purified merozoites when sequestration of schizonts occurs. 1, adipose tissue; 2, spleen; 3, liver; 4, lungs; 5, heart; 6, kidneys; 7, brain; 8, mammary fat pad; 9, muscles, and 10, testis; see also Figs. 9, 10, and 11. (*A*) Control CD36$^{+/+}$ WKY rat (*i*, 30 s; *iii*, 60 s; and *v*, 30 s) and CD36-deficient SHR rat (*ii*, 60 s; *iv*, 30 s; and *v*, 30 s). (*B*) Control CD36$^{+/+}$ (*i*, 30 s; *iii*, 30 s; and *v*, 10 s) and CD36$^{-/-}$ C57BL/6 mice (*ii*, 30 s; *iv*, 30 s; and *v*, 10 s). (*C*) Quantification of the luciferase activity in different organs by using the programs LIVING IMAGE and IGOR PRO. Photon counts from intact organs (dissected at 22 h) were expressed as the percentage of the total photon counts of all organs (relative luminescence); shaded box, Swiss mice; black box, control CD36$^{+/+}$, and open box: CD36$^{-/-}$ mice. (*Inset*) The percentage of schizonts in the peripheral blood (tail blood) circulation of the total number of schizonts present in the animals at 22 h. % RLU, percentage of relative luminescence.

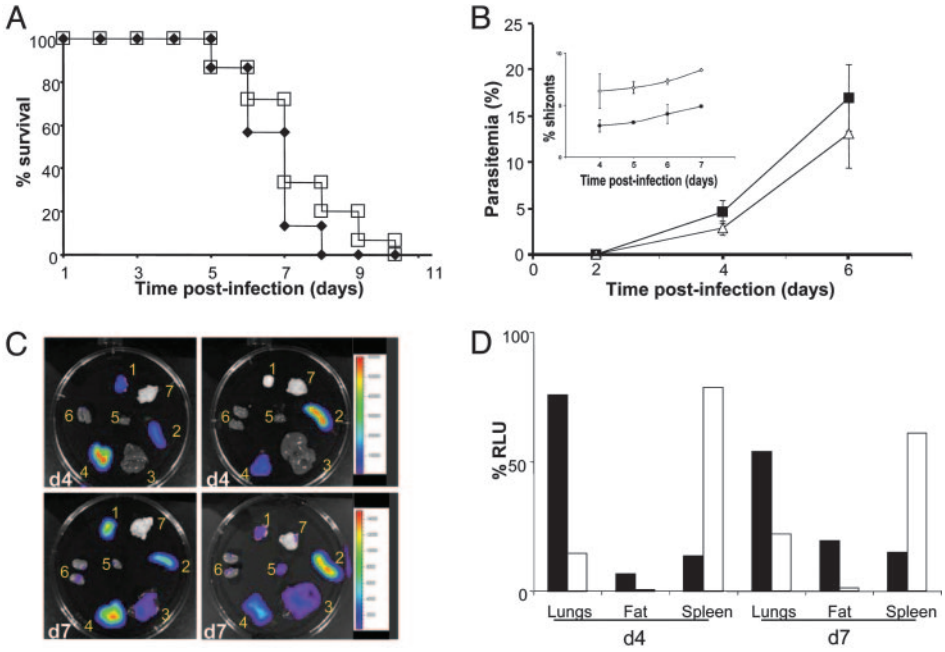

Fig. 5. Cerebral complications and sequestration of *P. berghei* in asynchronous infections in CD36$^{+/+}$ and in CD36$^{-/-}$ C57BL/6 mice. (*A*) Cumulative death of groups of mice as a result of cerebral complications (◆, CD36$^{+/+}$; □, CD36$^{-/-}$) in three experiments. (*B*) The course of parasitemia. (*Inset*) The percentage of schizonts in total irbc in the peripheral blood (tail blood) of control CD36$^{+/+}$ and CD36$^{-/-}$ mice infected with 10^5–10^6 parasites (■, CD36$^{+/+}$; △, CD36$^{-/-}$). (*C*) The distribution of schizonts (PbGFP-LUC$_{SCH}$) as visualized by measuring luciferase activity in dissected organs by using an I-CCD video camera (IVIS, Xenogen). Measurements were performed at days 4 and 7 after infection (10 s). 1, adipose tissue; 2, spleen; 3, liver; 4, lungs; 5, heart; 6, kidneys; and 7, brain. (*D*) Quantification of the luciferase activity (%RLU, percentage of relative luminescence) in different organs (dissected at day 4 or day 7 after infection) of control CD36$^{+/+}$ (black box) and CD36$^{-/-}$ (open box) C57BL/6 mice; see also Figs. 10–12.

web site), and the increased numbers of schizonts in the spleens of CD36$^{-/-}$ mice (Fig. 5 *B* and *D*).

Discussion

This report of *in vivo* imaging of malaria parasites in live animals demonstrates that luciferase-based imaging technology can be used to visualize parasite distribution in hosts and investigates parasite–host interactions. Using this method, we demonstrate the accumulation of *P. berghei* ANKA schizonts in the spleen and lungs, as has been shown for rodent malaria parasites in refs. 26 and 27, and a major site of sequestration in adipose tissue. We observed no sequestration of *P. berghei* in the brain, consistent with both low or absent expression of CD36 on the capillary endothelial cells of brain tissue (25, 28) and the low level of parasite sequestration in *P. berghei* CM models (7, 25). Murine CM has been associated mainly with the sequestration and activation of leukocytes and platelets in brain tissue (25, 29), in contrast to human CM, which is considered to be associated mostly with the sequestration of *P. falciparum* irbc in the brain. However, the field is controversial; some authors have shown the accumulation of parasites in the brain in murine malaria, whereas others have emphasized a potential role for leukocyte sequestration in the brain in human CM (30, 31). Using CD36$^{-/-}$ mice, we also show that almost all, if not all, irbc sequestration requires this molecule. In fact, CD36$^{-/-}$ mice no longer show irbc sequestration in lungs or adipose tissue. In both human and primate malaria, sequestration in adipose tissue has been reported (32–35), but, surprisingly, no detailed studies on the extent and importance of this tissue or the ligand/receptor interactions involved in sequestration have been performed. However, CD36 is abundantly expressed on the surface of the capillary endothelial cells of adipose tissue (28, 36). In contrast, the accumulation of *P. berghei* schizonts in the spleen appears not to be influenced by CD36 and might result from nonspecific accumulation or interactions with additional host receptors (either as a prelude to active removal of infected cells or active sequestration). The observed increase in parasites trapped in the spleen and the slower increase in parasite numbers in the CD36$^{-/-}$ mice indicate that CD36-mediated sequestration is beneficial for parasite survival in the host, as has been suggested in refs. 4 and 9. The general role of CD36 as a major receptor for the adherence of *P. falciparum*-irbc to endothelial cells is well established. CD36 is also considered to have a major role in nonopsonic phagocytosis of irbc by monocytes/macrophages and dendritic cells, for either human or murine malaria parasites (12). CD36-mediated nonopsonic phagocytosis leads to the down-modulation of inflammatory responses by these cells and, therefore, is thought to inhibit immune responses against the parasite (37). This report on the *in vivo* relevance of CD36 shows the importance of CD36 in *P. berghei* sequestration and its specific role in sequestration in adipose and lung tissues. Human and rodent CD36 are >90% identical at the amino acid level, and both support the cytoadherence of *P. falciparum*-irbc (38). Taken together with the demonstration that another rodent malaria parasite *Plasmodium chabaudi* binds human CD36 (39), the data suggest that binding to CD36 is an "ancient" feature of the *Plasmodium* genus and may indicate that rodent parasites modulate the surface of irbc, perhaps through the active export of proteins that contain as yet unidentified and potentially conserved binding domains that might also expand the type and range of *P. falciparum* adhesins. Currently, only the individual DBL and CIDR domains of the PfEMP1 protein family are known to be responsible for recognition of the various human endothelial receptors, but this protein family is not found in *Plasmodium vivax* and the rodent malarias. These latter parasites do possess and express a limited repertoire of contextually distinct DBL domains exclusively associated with erythrocyte recognition by the merozoite and not expressed on the irbc

surface for sequestration (40). The possible presence of a family of conserved adhesins associated with sequestration and of previously uncharacterized sites of sequestration, as described in this study, may require a reevaluation of the nonsequestering status of other human malaria parasites such as *P. vivax*. Indeed, splenic barrier cells have been proposed as a site of sequestration for *P. vivax*, which shares multigene families encoding irbc surface proteins (e.g., VIR and BIR) with *P. berghei* (41).

More importantly, this report dissociates irbc sequestration from CM pathology. Although the results clearly show that, in *P. berghei* ANKA infection, CD36 is required for irbc sequestration, $CD36^{-/-}$ mice still develop CM. Therefore, CD36-mediated sequestration in nonerythroid organs is not the basis of CM in murine models. With cautious extrapolation from rodent models to human infections, the data presented here challenge the widespread idea that irbc sequestration is a major cause of CM, a concept that needs to be taken into consideration when developing vaccines that aim to target the adhesion of *P. falciparum* irbc to endothelial cells (37). Our observations support the hypothesis that CM is an inflammatory-like syndrome (42) that can occur without sequestration of irbc (43), possibly as a consequence of parasite toxin (for example, the parasite gpi anchor) release during schizont rupture. Still, the involvement of CD36-mediated sequestration in other pathological aspects of severe malaria remains unknown. For example, respiratory distress is a major cause of death by severe malaria in endemic areas (44), and our results show that the lung is an important organ for CD36-mediated sequestration. Whether this pathology is associated with lung sequestration or is an inflammatory syndrome independent of irbc sequestration remains to be elucidated.

Although a direct role for CD36-mediated sequestration in the development of severe and cerebral *P. falciparum* malaria has been questioned, the issue is not fully resolved, and further investigation is warranted (9, 25, 45–48). The visualization technology reported here, in combination with transgenic *P. berghei* parasites expressing known adhesin domains of *P. falciparum* and transgenic mice with additional human endothelial cell receptors (e.g., ICAM-1) (49), may serve as a small-animal model for the *in vivo* screening of inhibitors of *P. falciparum* irbc sequestration. Furthermore, in combination with immunodeficient mouse models with specifically engineered lesions in the immune response pathways, *in vivo* parasite visualization may help unravel the complexities of parasite–host interactions that lead to the pathology observed in *P. falciparum*-infected humans and provide a basis for the development of therapies.

We thank Frans Prins and the personnel of the Leiden University Medical Center animal facility for excellent technical support. M.M.M. is the recipient of a European Molecular Biology Organization Young Investigator Award, and M.C.-R. is supported by Fundação para a Ciência e Tecnologia (Portugal) Fellowship SFRH/BD/8435/2002. This work was supported by the University of Leiden Stimuleringsfonds, the Wellcome Trust Functional Genomics Initiative, and European Community Grant EU INCO-DEV ICA4-1999-10022.

1. Ho, M. & White, N. J. (1999) *Am. J. Physiol.* **276,** C1231–C1242.
2. Sherman, I. W., Eda, S. & Winograd, E. (2003) *Microbes Infect.* **5,** 897–909.
3. Chotivanich, K., Udomsangpetch, R., McGready, R., Proux, S., Newton, P., Pukrittayakamee, S., Looareesuwan, S. & White, N. J. (2002) *J. Infect. Dis.* **185,** 1538–1541.
4. Engwerda, C. R., Beattie, L. & Amante, F. H. (2005) *Trends Parasitol.* **21,** 75–80.
5. Mackintosh, C. L., Beeson, J. G. & Marsh, K. (2004) *Trends Parasitol.* **20,** 597–603.
6. de Souza, J. B. & Riley, E. M. (2002) *Microbes Infect.* **4,** 291–300.
7. Hunt, N. H. & Grau, G. E. (2003) *Trends Immunol.* **24,** 491–499.
8. Pasvol, G. (2001) *Clin. Med.* **1,** 495–500.
9. Serghides, L., Smith, T. G., Patel, S. N. & Kain, K. C. (2003) *Trends Parasitol.* **19,** 461–469.
10. Ockenhouse, C. F., Tandon, N. N., Magowan, C., Jamieson, G. A. & Chulay, J. D. (1989) *Science* **243,** 1469–1471.
11. Urban, B. C., Ferguson, D. J., Pain, A., Willcox, N., Plebanski, M., Austyn, J. M. & Roberts, D. J. (1999) *Nature* **400,** 73–77.
12. Urban, B. C., Willcox, N. & Roberts, D. J. (2001) *Proc. Natl. Acad. Sci. USA* **98,** 8750–8755.
13. Koning-Ward, T. F., Janse, C. J. & Waters, A. P. (2000) *Annu. Rev. Microbiol.* **54,** 157–185.
14. Aitman, T. J., Glazier, A. M., Wallace, C. A., Cooper, L. D., Norsworthy, P. J., Wahid, F. N., Al Majali, K. M., Trembling, P. M., Mann, C. J., Shoulders, C. C., *et al.* (1999) *Nat. Genet.* **21,** 76–83.
15. Collison, M., Glazier, A. M., Graham, D., Morton, J. J., Dominiczak, M. H., Aitman, T. J., Connell, J. M., Gould, G. W. & Dominiczak, A. F. (2000) *Diabetes* **49,** 2222–2226.
16. Febbraio, M., Abumrad, N. A., Hajjar, D. P., Sharma, K., Cheng, W., Pearce, S. F. & Silverstein, R. L. (1999) *J. Biol. Chem.* **274,** 19055–19062.
17. Goudriaan, J. R., Dahlmans, V. E., Teusink, B., Ouwens, D. M., Febbraio, M., Maassen, J. A., Romijn, J. A., Havekes, L. M. & Voshol, P. J. (2003) *J. Lipid Res.* **44,** 2270–2277.
18. Chatterjee, S., Ngonseu, E., Van Overmeir, C., Correwyn, A., Druilhe, P. & Wery, M. (2001) *Afr. J. Med. Med. Sci.* **30,** 25–33.
19. Mons, B., Janse, C. J., Boorsma, E. G. & Van der Kaay, H. J. (1985) *Parasitology* **91,** 423–430.
20. Janse, C. J. & Waters, A. P. (1995) *Parasitol. Today* **11,** 138–143.
21. Curfs, J. H., Schetters, T. P., Hermsen, C. C., Jerusalem, C. R., van Zon, A. A. & Eling, W. M. (1989) *Clin. Exp. Immunol.* **75,** 136–140.
22. Hermsen, C. C., Crommert, J. V., Fredix, H., Sauerwein, R. W. & Eling, W. M. (1997) *Parasite Immunol.* **19,** 571–577.
23. Collette, A., Bagot, S., Ferrandiz, M. E., Cazenave, P. A., Six, A. & Pied, S. (2004) *J. Immunol.* **173,** 4568–4575.
24. Beetsma, A. L., van de Wiel, T. J., Sauerwein, R. W. & Eling, W. M. (1998) *Exp. Parasitol.* **88,** 69–72.
25. Patel, S. N., Serghides, L., Smith, T. G., Febbraio, M., Silverstein, R. L., Kurtz, T. W., Pravenec, M. & Kain, K. C. (2004) *J. Infect. Dis.* **189,** 204–213.
26. Smith, L. P., Hunter, K. W., Oldfield, E. C. & Strickland, G. T. (1982) *Infect. Immun.* **38,** 162–167.
27. Coquelin, F., Boulard, Y., Mora-Silvera, E., Richard, F., Chabaud, A. G. & Landau, I. (1999) *C. R. Acad. Sci. Ser. III* **322,** 55–62.
28. Greenwalt, D. E., Scheck, S. H. & Rhinehart-Jones, T. (1995) *J. Clin. Invest.* **96,** 1382–1388.
29. Grau, G. E., Tacchini-Cottier, F., Vesin, C., Milon, G., Lou, J. N., Piguet, P. F. & Juillard, P. (1993) *Eur. Cytokine Network* **4,** 415–419.
30. Patnaik, J. K., Das, B. S., Mishra, S. K., Mohanty, S., Satpathy, S. K. & Mohanty, D. (1994) *Am. J. Trop. Med. Hyg.* **51,** 642–647.
31. Hearn, J., Rayment, N., Landon, D. N., Katz, D. R. & de Souza, J. B. (2000) *Infect. Immun.* **68,** 5364–5376.
32. Miller, L. H. (1969) *Am. J. Trop. Med. Hyg.* **18,** 860–865.
33. Miller, L. H. (1970) *J. Parasitol.* **56,** 1028–1029.
34. Miller, L. H., Fremount, H. N. & Luse, S. A. (1971) *Am. J. Trop. Med. Hyg.* **20,** 816–824.
35. Wilairatana, P., Riganti, M., Puchadapirom, P., Punpoowong, B., Vannaphan, S., Udomsangpetch, R., Krudsood, S., Brittenham, G. M. & Looareesuwan, S. (2000) *Southeast Asian J. Trop. Med. Public Health* **31,** 203–212.
36. Febbraio, M., Hajjar, D. P. & Silverstein, R. L. (2001) *J. Clin. Invest.* **108,** 785–791.
37. Duffy, P. E., Craig, A. G. & Baruch, D. I. (2001) *Trends Parasitol.* **17,** 354–356.
38. Serghides, L., Crandall, I., Hull, E. & Kain, K. C. (1998) *Blood* **92,** 1814–1819.
39. Mota, M. M., Jarra, W., Hirst, E., Patnaik, P. K. & Holder, A. A. (2000) *Infect. Immun.* **68,** 4135–4144.
40. Blair, P. L., Kappe, S. H., Maciel, J. E., Balu, B. & Adams, J. H. (2002) *Mol. Biochem. Parasitol.* **122,** 35–44.
41. del Portillo, H. A., Lanzer, M., Rodriguez-Malaga, S., Zavala, F. & Fernandez-Becerra, C. (2004) *Int. J. Parasitol.* **34,** 1547–1554.
42. Clark, I. A. & Rockett, K. A. (1994) *Parasitol. Today* **10,** 410–412.
43. Berendt, A. R., Tumer, G. D. & Newbold, C. I. (1994) *Parasitol. Today* **10,** 412–414.
44. Marsh, K., English, M., Crawley, J. & Peshu, N. (1996) *Ann. Trop. Med. Parasitol.* **90,** 395–402.
45. Rogerson, S. J., Tembenu, R., Dobano, C., Plitt, S., Taylor, T. E. & Molyneux, M. E. (1999) *Am. J. Trop. Med. Hyg.* **61,** 467–472.
46. Aitman, T. J., Cooper, L. D., Norsworthy, P. J., Wahid, F. N., Gray, J. K., Curtis, B. R., McKeigue, P. M., Kwiatkowski, D., Greenwood, B. M., Snow, R. W., *et al.* (2000) *Nature* **405,** 1015–1016.
47. Traore, B., Muanza, K., Looareesuwan, S., Supavej, S., Khusmith, S., Danis, M., Viriyavejakul, P. & Gay, F. (2000) *Am. J. Trop. Med. Hyg.* **62,** 38–44.
48. Pain, A., Ferguson, D. J., Kai, O., Urban, B. C., Lowe, B., Marsh, K. & Roberts, D. J. (2001) *Proc. Natl. Acad. Sci. USA* **98,** 1805–1810.
49. Dufresne, A. T. & Gromeier, M. (2004) *Proc. Natl. Acad. Sci. USA* **101,** 13636–13641.